Analysis of the spectral and angular response of the vegetated surface polarization for the purpose of aerosol remote sensing over land

F. Waquet,[1,*] J.-F. Léon,[1] B. Cairns,[2] P. Goloub,[1] J.-L. Deuzé,[1] and F. Auriol[1]

[1]Laboratoire d'Optique Atmosphérique, UMR 8518 CNRS, Université des Sciences et Technologies de Lille, 59655 Villeneuve-d'Ascq CEDEX, France

[2]NASA Goddard Institute for Space Studies, 2880 Broadway, New York, New York 10025, USA

*Corresponding author: waquet@loa.univ-lille1.fr

Received 22 July 2008; revised 12 January 2009; accepted 16 January 2009; posted 16 January 2009 (Doc. ID 99181); published 19 February 2009

A precise estimate of the polarization induced by the surface in reflected radiation is crucial for remote sensing applications dedicated to monitoring the atmosphere. Here we present airborne observations acquired during a field campaign in the North of France over vegetated surfaces. Polarized reflectances were measured in four spectral bands in the range between 0.67 and 2.2 μm and for scattering angles between 75° and 145°. Our results confirm that the polarization generated by the reflection of vegetated surfaces can be understood as being primarily a specular reflection process. It is not possible from our measurements to see any spectral dependence of the surface polarization in the given spectral channels. The surface polarization is well fitted by existing surface models which have two degrees of freedom that allow the magnitude and angular behavior of the surface-polarized reflectance to be adjusted.

OCIS codes: 120.0280, 280.1100, 120.6660, 120.5410.

1. Introduction

Aerosol particles in the atmosphere can affect the radiation balance of the earth–atmosphere system by reflecting and absorbing sunlight and absorbing and emitting infrared radiation. Moreover, aerosols play a crucial role in the lifecycle and optical properties of clouds. Climate change estimations consider both a direct effect of aerosols on radiation budget and an indirect effect through the interaction with clouds. Current estimation of the magnitude and sign of the aerosol impact on climate is still an issue because of large remaining uncertainties [1].

During the past decade, the development of spaceborne remote sensing has provided a considerable amount of observations on aerosol load and properties at the global scale [2,3]. Spaceborne radiometers make use of the reflected sunlight by the earth–atmosphere system in specific spectral bands to determine the aerosol optical properties. The retrieval of aerosol parameters is affected by the optical properties of the underlying surface. Indeed one of the main difficulties in aerosol remote sensing from space in the solar spectrum remains in separating the aerosol contribution from that of the surface [4]. Over ocean, the surface is dark enough in the shortwave spectrum to not mask the atmospheric signal. Over land surfaces, the albedo depends strongly on the land surface type and vegetation cover and is one of the largest uncertainties in the aerosol optical depth retrieval [5].

The albedo of dark dense vegetation is low enough to enable the retrieval of aerosol optical thickness (AOT) [6]. When considering a large ratio of the wavelength to the size of the particle, the atmosphere tends to be thin, and then the surface can be observed. Kaufman *et al.* [7] used a channel at

0003-6935/09/061228-09$15.00/0

2.2 μm to evaluate the surface reflectance. This estimation is then extrapolated to shorter wavelengths using empirical color ratios [8]. As shown in [9], those ratios are weakly dependent on the viewing and illumination geometry. However, the use of fixed ratios might not be adequate for all kinds of surface and especially over urban or peri-urban areas [10,11]. With such a method, the accuracy in the retrieved aerosol optical depth remains, however, lower than for the retrieval over ocean surface [12]. In case of a multilook satellite radiometer, the angular response of the surface reflectance also has to be accounted for. The shape of the surface bidirectional reflectance distribution function reflects principally the interaction of light with the macrophysical structure of the surface, and therefore the variation with the wavelength is weak [13]. This property has been used in the retrieval of AOT from the dual-viewing sensor Along-Track Scanning Radiometer-2 [14,15] and the Multiangle Imaging Spectroradiometer [16].

Polarized measurements provide an alternative and robust approach for the study of aerosols over land. Indeed the polarized surface contribution is smaller than, or equal to, that of the atmosphere. Moreover it shows little spectral dependence and generally weak spatial contrast, except for cultivated land and in the transition between urban and natural surfaces [17,18]. The surface bidirectional polarized reflectance distribution function (BPDF) can be modeled using a simple mathematical formula based on Fresnel reflection law [17,19,20] and even adjusted using a semiempirical parametrization [21]. However, using a BPDF model to predict the surface-polarized reflectance can introduce significant uncertainties in the retrieval of the AOT. It is therefore desirable to have a direct estimate of the surface-polarized reflectance. However, the angular distribution of the surface-polarized reflectance cannot be directly measured in any geometry with a satellite sensor, and one needs to use a mathematical representation of the surface BPDF that fits the measurements and can be used for modeling surface–atmosphere interactions.

In a earlier paper [10], a new approach was developed to retrieve aerosol properties over land based on the use of multispectral polarized measurements provided by an airborne polarimeter called MICROPOL [22]. In this study, we used data acquired with the MICROPOL instrument during two regional airborne experiments that were atmospherically corrected in order to investigate the spectral dependence of the surface polarization and to test the ability of various BPDF models to reproduce the surface polarization angular behavior. The effects of differences between the surface models on the retrieved aerosol parameters were also discussed. This study follows on from other work [23,24] that used measurements provided by the airborne Research Scanning Polarimeter (RSP) [25] to study surface optical properties over a wide spectral and view angle range for various surface types.

2. Measurements and Modeling

The MICROPOL instrument is a single viewing angle multiwavelength airborne instrument that provides accurate measurements in five spectral bands centered on 0.49, 0.67, 0.87, 1.6, and 2.2 μm. Each spectral band is equipped with a set of three linear polarizers with polarization azimuths separated by an angle of 60°. The first three Stokes parameters, $[I, Q, U]$, are then derived from the measurements performed on each polarizer [22]. Here we use the normalized total and polarized radiances, L and Lp (W m^{-2} sr^{-1}) that are defined terms of the first three Stokes parameters $[I, Q, U]$ integrated over the particular spectral band to be,

$$L = \pi I / E_0, \tag{1}$$

$$Lp = \pi (Q^2 + U^2)^{1/2} / E_0. \tag{2}$$

In Eqs. (1) and (2), E_0 is the spectral solar extraterrestrial irradiance integrated over the spectral band of interest (W m^{-2}). In our data processing, the polarized radiance was signed positive when the polarization direction was perpendicular to the plane of scattering (the plane containing the solar and viewing directions) and signed negative when it was parallel to the plane of scattering. The total and polarized reflectances are computed by dividing the total and polarized normalized radiances by μ_s, the cosine of the solar zenith angle θ_s. The relative accuracy in polarized radiance is 2–3% for the spectral bands with center wavelengths of 0.49, 0.67, 0.865, and 1.6 μm and 6% for the 2.2 μm spectral band. We also note here that the symbols used in succeeding equations to represent the viewing zenith angles θ_v, the scattering angle Θ, and the relative azimuth angle φ_r (varying from 0° in the specular direction to 180° in the opposite direction).

The upward-polarized radiances measured at the instrument level z can be written in the following form [19,26]:

$$\begin{aligned} Lp_\lambda^{\mathrm{Meas}}(z, \theta_s, \theta_v, \varphi_r) &= Lp_\lambda^{\mathrm{Atm}}(z, \theta_s, \theta_v, \varphi_r) \\ &+ \mu_s . Rp_\lambda^{\mathrm{Surf}}(\theta_s, \theta_v, \varphi_r) . T_\lambda^{\downarrow}(\theta_s) . T_\lambda^{\uparrow}(z, \theta_v), \end{aligned} \tag{3}$$

where λ indicates that this equation has spectral dependence. $Lp_\lambda^{\mathrm{Atm}}$ is the polarized radiance for an atmosphere above a black surface (i.e., polarized path radiance). $Rp_\lambda{}^{\mathrm{surf}}$ corresponds to the bidirectional polarized reflectance factor (BPF) of the surface (unitless). The BPF is defined as the bidirectional reflectance factor of a target [27] but for the fraction of the reflected radiation that is polarized. The term "surface-polarized reflectance" used in this paper refers to this quantity observed for a particular illumination direction. $T_\lambda^{\downarrow}$ and $T_\lambda^{\uparrow}$ are, respectively, the downward and upward transmission terms and are computed using the following equations:

$$T_\lambda^{\downarrow}(\theta_s) = \exp\left[-\left(\frac{\psi\delta_{o,\lambda}^{m} + \varsigma\delta_{o,\lambda}^{a}}{\mu_s}\right)\right], \quad (4)$$

$$T_\lambda^{\uparrow}(z,\theta_v) = \exp\left[-\left(\frac{\psi\delta_{\lambda}^{m}(z) + \varsigma\delta_{\lambda}^{a}(z)}{\mu_v}\right)\right], \quad (5)$$

where μ_v is the cosine of the viewing zenith angle, the superscript indicates whether we are considering aerosols ($x = a$) or molecules ($x = m$), and $\delta_{0,\lambda}^{x}$ is the optical thickness of the atmosphere, whereas the optical thickness at the instrument level z is given by

$$\delta_\lambda^x(z) = \delta_{o,\lambda}^x(1 - \exp(-z/H_x)). \quad (6)$$

The molecular optical thickness is calculated following Hansen and Travis [28]. The molecular scale height, H_m, is set to the standard value of 8 km, and the aerosol scale height, H_a, is 2 km, which is a typical value for aerosols in the boundary layer. The aerosol optical properties are computed assuming homogeneous spherical particles for which the Mie theory is used to calculate the scatter of light. The atmospheric polarized radiance $Lp_\lambda^{\mathrm{Atm}}$ is accurately estimated using the successive order of scattering code [29]. Equation (3) does not account for the diffuse interactions between the surface and the atmosphere explicitly but rather by using a set of coefficients ψ and ζ in Eqs. (4) and (5) [17,30]. ψ is equal to 0.9, and ζ depends on the aerosol model and is derived using an empirical relation [31]:

$$\varsigma = 0.3658 + 0.1023\alpha^* + 0.0080\alpha^{*2}, \quad (7)$$

where α^* is the Ångström parameter defined using the AOTs at 0.670 and 0.865 μm [26]. Lafrance *et al.* [31] estimated that Eq. (3) allows one to model the polarized reflectance with an absolute accuracy better than 2.10^{-4} for AOT smaller than 0.1 at 0.67 μm and for view and illumination angles smaller than 60°. The accuracy of Eq. (3) decreases for increasing optical thickness. For this reason the channel at 0.49 μm is not included in the present study. The operational inversion algorithm [30] developed for the AERONET/PHOTONS sun photometers provides the aerosol burden and the aerosol microphysical properties. These quantities are used to estimate the AOT in Eqs. (4) and (5) and to calculate the path radiance in Eq. (3). The surface-polarized reflectance is then estimated by substituting Eqs. (4)–(6) into Eq. (3) and solving for that quantity.

Many experimental studies have shown that the surface-polarized reflectance is mainly generated by single reflection of the incident radiation at surface facets (e.g., grains of sand and cuticles of leaves) [32]. Based on this consideration, different surface BPDF models have been developed for vegetation covers [20,33] or bare soils [17]. The surface is then conceptualized as an agglomeration of separate objects of similar shape that are randomly oriented. The models developed for vegetated covers account for the attenuation of the incident beam by transmission through the cover as well as the effects of shadowing of leaves. Assuming a uniform orientation of the leaf inclination (i.e., isotropically oriented surface facets), a simplified expression of the surface-polarized reflectance R_p^{surf} for dense vegetation is given by Bréon *et al.* [17]:

$$R_p^{\mathrm{surf}}(\theta_s,\theta_v,\varphi_r) = \frac{F_p(\gamma)}{4(\mu_s + \mu_v)}, \quad (8)$$

where γ is the incident angle on the reflected element, $\gamma = (\pi - \Theta)/2$, and F_p is the Fresnel coefficient for polarized light generated by surface reflection of an unpolarized direct incident beam.

A surface BPDF model for bare soil was proposed by Bréon *et al.* [17]. The bare soil is assimilated to a rough surface, where the facets of the individual objects are isotropically oriented. The shadowing effects are neglected, and there are no transmission terms, as for the model previously described. The surface-polarized reflectance R_p^{surf} is then written as

$$R_p^{\mathrm{surf}}(\theta_s,\theta_v,\varphi_r) = \frac{F_p(\gamma)}{4\mu_s.\mu_v}. \quad (9)$$

Cairns *et al.* [19] presented an alternative to the previous model by using a factor that accounts for the neglect of the mutual shadowing of facets. Assuming a Gaussian distribution of the surface slopes, this shading factor is given by Saunders *et al.* [34]:

$$S(\theta) = \frac{2}{1 + \mathrm{erf}(\nu) + \left(\nu\sqrt{\pi}\right)^{-1}\exp(-\nu^2)}, \quad (10)$$

where

$$\nu = \left(\sigma\sqrt{2}\right)^{-1}\tan(\theta), \quad (11)$$

with σ^2 being the mean square slope value, which is related to the surface roughness. The surface-polarized reflectance is corrected using this shadowing factor for both the viewing and illumination angles.

From the observations collected by the POLDER instrument between November 1996 and June 1997, Nadal and Bréon [21] developed a semiempirical model of the surface-polarized reflectance:

$$R_p^{\mathrm{surf}}(\theta_s,\theta_v,\varphi_r) = \alpha\left[1 - \exp\left(-\beta\frac{F_p(\gamma)}{\mu_s + \mu_v}\right)\right], \quad (12)$$

where α and β are empirical coefficients that are determined by the Normalized Difference Vegetation Index (NDVI) of the observed surface and the ground-type classification given by the International Geosphere and Biosphere Project (IGBP) for that

particular location. The IGBP ground-type classification includes 17 different surface classes called "geotypes." Some of these surface classes are subdivided into NDVI classes [21], leading to a total of 27 different surface classes. This land classification is given for a resolution of 20 km × 20 km.

It should also be noted that a linear combination of Eqs. (8) and (9) has been also used in polarimetric aerosol remote sensing applications [18,35].

In any of those models, the spectral dependence is provided by the Fresnel coefficient term. Indeed, for a given viewing geometry, the polarized Fresnel coefficient F_p only depends on the surface refractive index. The refractive index of natural surfaces remains poorly documented. A commonly accepted value of 1.5 is used for any kind of surface, even if it might be not appropriate for an urban surface [36]. However, according to the literature, this parameter shows little spectral variation for natural matter between 0.4 and 2 μm [33,37], with the consequence that the surface-polarized reflectance should have similarly weak spectral dependence over a wide spectral range.

3. Description of the Data

Between October 2002 and October 2005, seven flights were performed with the MICROPOL instrument integrated onto a lightweight aircraft in the North of France. Among these flights we have selected two that correspond to low aerosol loading conditions in order to investigate the surface optical properties. A digital camera was associated with the MICROPOL instrument in order to identify the overflown surfaces. These flights were performed close to the AERONET/PHOTONS sun photometer located close to the city of Lille (50.61 °N, 3.14 °E). The main characteristics of the flights are summarized in Table 1.

The first flight consisted of a simple northward flight track segment of 30 km centered on the sun photometer ground-based station. Figure 1 shows an example of polarized reflectance measured during the first flight at an altitude of 3.5 km and as a function of the UT of acquisition. The measurements were acquired with a stable viewing geometry, and the fluctuations observed in the polarized radiances are the result of variability in the physical and optical properties of the overflown surfaces. The measured polarized reflectance decreases with wavelength, as expected, if the surface polarization has a weak spectral dependence, since the atmospheric scattering (mainly generated by molecules here) decreases with wavelength.

During this transect the overflown surfaces are representative of typical landscapes observed in the North of France, which are mainly composed of open fields, cropland, and a few sparsely separated manmade objects such as roads and villages. The aircraft passed over the sun photometer between 12.47 and 12.48 UT. At this time we observe an increase in the polarized reflectances measured in each spectral band that corresponds to the transition between vegetated and urbanlike surfaces. We assume that the characteristics of the urban surface (e.g., macrostructure, materials, and smoothness of the surfaces) are responsible for the high levels of polarization.

The second flight consisted of a flight track segment between the cities of Lille and Valenciennes, located 35 km southeast of Lille. During this flight we flew over a forest area as well as the same types of surface that were observed during the first flight. The forest areas are characterized by values of the NDVI that are larger than 0.75, whereas croplike surfaces are associated with values of the NDVI ranging between 0.4 and 0.75. This flight was performed at a low altitude in order to minimize the atmospheric effects on the measurements. We consider that, for this case, the contribution of the atmospheric layer below the aircraft can be neglected and that a simplified correction based on Eq. (3) can be used. In effect, the quantities $Lp_\lambda^{\mathrm{Atm}}$ and $T_\lambda^{\uparrow}$ in Eq. (3) were set to 0 and 1, respectively, when this equation was solved for the surface-polarized reflectance. The MICROPOL measurements were therefore only corrected for the downward transmission term. During the second flight, several overpasses over the same flight track segment were performed for different viewing angles. This data set was used to simulate multidirectional observations in order to

Table 1. Main Characteristics of the Flights[a]

Flight Number	Date and Time (UT)	$\delta^a_{0.0.67}$	Aircraft Altitude (km)	Viewing Geometry	Comments
1	18 February 2003; 12:00–13:00	0.045 (0.005)	3.5	$\theta_s = 63°$ (±1); $\theta_v = 0°$ or 45°; $\varphi_r = 6°$ (±4); $\Theta = 120°$ or 75°	Very clear sky condition. Only two viewing geometries. Mainly cropped surfaces and a few urban areas overflown. Diameter footprint of 0.12 km.
2	31 August 2005; 8:45–10:15	0.07 (0.01)	0.2	$\theta_s = 50°$ (±5); $\varphi_r = 0°$ (±20); $\theta_v = 45, 30, 15, 5, -5, -15$; $80° < \Theta < 145°$	Forest, closely cropped surfaces, and a few urban areas overflown. Eight viewing geometries. Diameter footprint of 0.12 km.

[a] $\delta^a_{0.0.67}$ is the mean AOT at 0.67 μm, measured during the flight; the associated standard deviation is reported in the parentheses. The uncertainty on $\delta^a_{0.0.67}$ is equal to 0.01. The values given in brackets for θ_s and φ_r indicate the maximum variability observed during the flight.

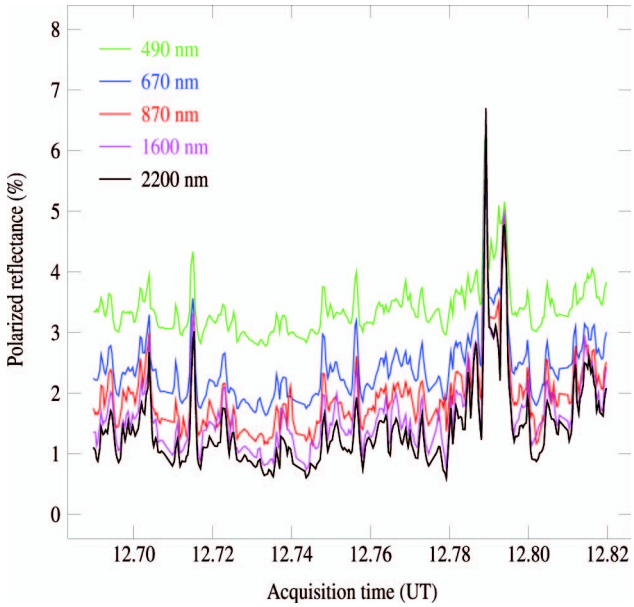

Fig. 1. Measured polarized radiance at an altitude of 3.5 km. The transect corresponds to a distance of 10 km. The measurements were acquired in the principal plan and for a scattering angle of approximately 75°.

evaluate the surface models developed for natural surfaces.

4. Results

A. Analysis of the Surface Polarization Spectral Response

The data acquired during the first flight were used to examine the spectral behavior of the observed surface at 0.67, 0.87, and 1.6 μm compared to 2.2 μm. Figure 2 shows the surface-polarized reflectance estimated in the 0.67, 0.87, and 1.6 μm bands as a function of the same quantity at 2.2 μm. We observe some dispersion of the measurements around the one-to-one line. This dispersion is caused by the spatial variability in the sampled surfaces (as one can see in Fig. 1) as well as instrumental noise. The parameters of the linear regression shown in Fig. 2 are reported in Table 2. The numbers in brackets correspond to the uncertainty in the regression parameters assuming an uncertainty in the AOT of ± 0.01, which corresponds to the accuracy of the sun photometer. We can observe very high interband correlations with a correlation coefficient above 0.92 for the spectral bands of the MICROPOL instrument. The slopes are close to 1, and the offsets are small, indicating that the mean spectral effects are weak. This first result shows that the surface-polarized reflectance is spectrally neutral, within the uncertainties caused by measurement noise and atmospheric correction, over a large spectral range (0.67–2.2 μm).

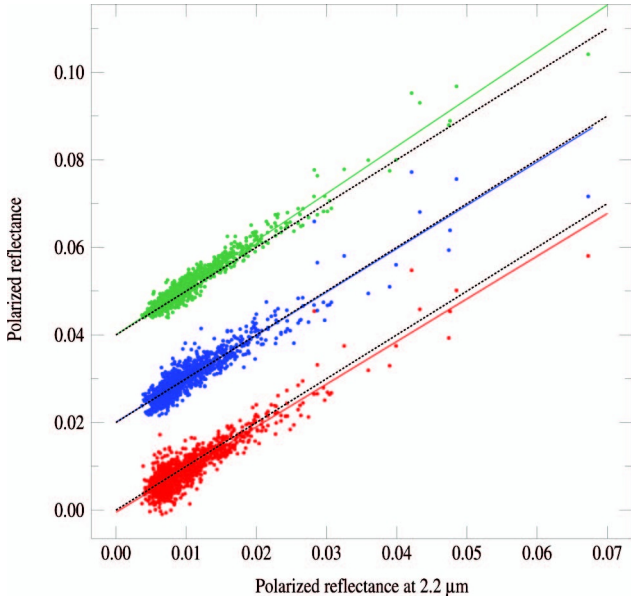

Fig. 2. Surface-polarized reflectance estimated at 0.87, 0.67, and 1.6 μm, respectively, in red, blue, and dark green, as a function of the same quantity at 2.2 μm for a forward-viewing geometry and a nadir view (flight 18 February 2003, see Table 1). The observations at 0.67 and 1.6 μm were offset by 0.02 and 0.04, respectively, for the sake of clarity.

The data of the flight performed at low altitude were used to estimate the spectral behavior of the surface-polarized reflectance for forest and closely cropped surfaces. We split the results into two surfaces classes based on their NDVI values. We estimated the uncertainties in the atmospheric correction and propagated those errors to determine that the uncertainties in the estimated surface-polarized reflectance are less than 2% at 0.67 μm and negligible at 2.2 μm. For the surface class corresponding to NDVI above 0.75 (forest), the differences between the polarized reflectance at 0.67 and 2.2 μm range between 1.5×10^{-3} and -1.5×10^{-3} for most of the measurements (>80%), and the average absolute difference (AAD) is equal to 2.5×10^{-4}. The spectral effects observed for this surface class are dispersed symmetrically around zero, which means that the surface-polarized reflectance of this surface type is spectrally neutral at least within the measurement noise of approximately 1.5×10^{-3}. Similar conclusions can be drawn for the surface class corresponding to NDVI values ranging between 0.4 and 0.75 (primarily fields) since we observed a small AAD of 5.5×10^{-4} and a similar measurement noise.

B. Modeling the Surface Polarization Angular Response

Here we evaluate the ability of different surface BPDF models to reproduce the observed surface polarization angular behavior. During the second flight, the surfaces were observed with several different view angles close to the principal plane, thus giving the opportunity to compare measurements and models over a fairly large range of scattering angles.

Figures 3(a) and 3(b) show a comparison between the surface-polarized reflectance derived from the MICROPOL measurements at 2.2 μm and the ones calculated with the different surface BPDF models presented in Subsection 4.C and other alternative models described hereafter. We reported a mean

Table 2. Parameters of the Linear Regression Performed in Fig. 2[a]

	0.67/2.2 μm	0.87/2.2 μm	1.6/2.2 μm
Slope	0.99 (0.04)	0.97 (0.04)	1.07 (0.01)
Offset	5.5×10^{-5} (4×10^{-3})	4.5×10^{-4} (3×10^{-4})	-1×10^{-5} (6×10^{-5})
Correlation Coefficient	0.92	0.91	0.97

[a]The uncertainties due to the atmospheric corrections are reported in the parentheses.

value (black squares) and the associated standard deviation (bars) calculated over the entire transect for each viewing geometry. We selected restricted NDVI classes within the forest and closely cropped surface classes. The first class is defined by the NDVI ranging between 0.4 and 0.45, and the second class is defined by the NDVI values ranging between 0.88 and 0.89. Within the latter class, we rejected the observations associated with total reflectance measurements at 2.2 μm larger than 0.05, which ensures that only dark dense vegetated targets are considered [7] and that the selected surface classes are associated with a comparable number of observations. Our measurements show that the surface-polarized reflectance for a given viewing geometry increases with decreasing NDVI values [21]. The surface-polarized reflectances shown in Figs. 3(a) and 3(b) then encompass many intermediate surface-polarized reflectance values measured over the 0.40–0.90 NDVI range. We have considered four different models. The first one (referred to as NB in Fig. 3 and in the text hereinafter) is based on the parameterization of Nadal and Bréon [21]. A least mean square regression is used to derive the coefficients α and β. The parameters of the surface models are only fitted using the measurements at 2.2 μm. The second model (referred to as VB) is a weighted sum of the models proposed by Bréon *et al.* [17] for vegetated [Eq. (8)] and bare soils [Eq. (9)]. The relative weight between vegetated and bare soil is also adjusted by a least mean square fit. The third model (referred to FR) is directly proportional to the Fresnel reflectance (i.e., $R_p^{\mathrm{Surf}} = \xi \times F_p(\gamma)$), where ξ is adjusted to provide the best fit with the measurements. The last model is the same as model FR, except that it includes the shading factor defined in Eq. (10) (i.e., $R_p^{\mathrm{Surf}} = \xi \times F_p(\gamma) \times S(\theta_s) \times S(\theta_v)$). The mean square slope that drives the shading factor S is also included in the regression (referred to as FRS in the Fig. 3).

We observe in Figs. 3(a) and 3(b) that the surface-polarized reflectance decreases with the scattering angle and that the proposed models all agree qualitatively with the observed behavior. This is consistent with previous studies that have shown that the Fresnel law is the primary determinant of the surface-polarized reflectance over land.

We first describe the results obtained for the 0.40–0.45 NDVI class surface (closely cropped surfaces) shown in Fig. 3(a). The NB model matches the measurements quite well with α and β, respectively, equal to 1.17×10^{-2} and 53. The location where the measurements were made corresponds to the geotype 12, labeled as "*crops*," for which the coefficients α and β in the global model of Nadal and Bréon [21] are equal to 1.53×10^{-2} and 56, respectively. The fitted coefficients are closer to those taken for the geotype 14, labeled as "*natural_vegetation*" ($\alpha = 1.09 \times 10^{-2}$ and $\beta = 63$), that is also observed in the North of France. The use of the predefined coefficients from the global model leads to significant departures between measurements and model as large as 3.5×10^{-3} for geotype 12 and 0.25×10^{-3} for geotype 14 (not shown).

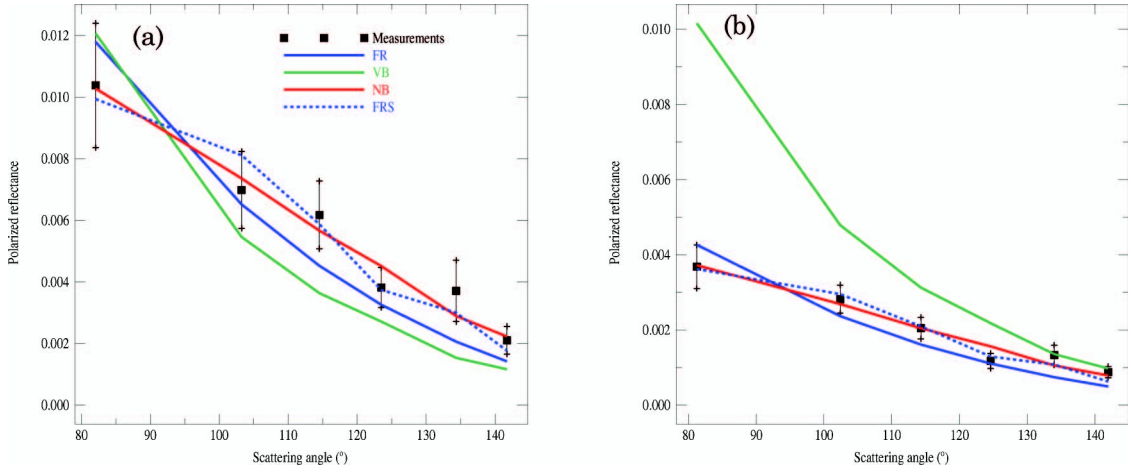

Fig. 3. (a) Surface-polarized reflectance measured over closely cropped surfaces as a function of the scattering angle: mean values (squares) and associated standard deviations (bars). The different models are described in the text. (b) Surface-polarized reflectance measured over forest area as a function of the scattering angle: mean values (squares) and associated standard deviations (bars).

When combining the vegetation and bare soil models (VB model), the best fit is found for a fraction of 0.895 for the vegetation. This model significantly underestimates the measured surface-polarized reflectance over a large range of scattering angle (100–140°). The third model (FR model) is the Fresnel polarized coefficient scaled by a coefficient ξ. The coefficient ξ roughly accounts for the intrinsic properties of the surface (e.g. smoothness and shadowing). It also accounts for the surface refractive index since the Fresnel reflectance calculated for one refractive index is proportional to a good degree of approximation to that calculated for a different refractive index. In our case, the best fit is found for $\xi = 0.23$. This model fits the observations within the standard deviation values for half the sampled viewing geometries. The FRS model allows reproducing the measurements within the standard deviation values with ξ and σ, respectively, equal to 0.5 and 1.75.

The same method has been applied to the 0.88–0.89 NDVI class (forest). The regressions are reported in Fig. 3(b). The NB model fits the measurements within the given standard deviations, except for one viewing geometry (scattering angle of approximately 125°). The α and β coefficients are, respectively, equal to 6.6×10^{-3} and 43. The geotype that provides the coefficients closest to these values corresponds to the geotype five, labeled as "*forest*" ($\alpha = 8.5 \times 10^{-3}$ and $\beta = 77$). The regression on the VB model leads to a fraction of 1.0 of the vegetated surface model, and for this model we observe an overestimate of the surface-polarized reflectance at small scattering angles. Our simple model (FR) is still robust in modeling the observed angular behavior of the surface-polarized reflectance and fits half the observations within the standard deviations. Finally the FRS model matches the data for fit parameters of $\xi = 0.175$ and $\sigma = 1.71$.

C. Impacts of the Surface Model on the Retrieved Aerosol Parameters

Here we used the retrieval approach described by Waquet *et al.* [38] to evaluate the effects of the differences between the surface models on the retrieved aerosol parameters.

We simulated polarized reflectance measurements in seven spectral bands (410, 470, 550, 670, 865, 1600, and 2250 nm) for an aerosol model defined by a single lognormal size distribution with an effective radius, r_{eff}, of 0.149 μm and an effective variance, v_{eff}, of 0.1735. We use a complex refractive index (m) of $1.47 - 0.01i$. The aerosol single scattering albedo, ω_0, is equal to 0.93 at 670 nm, and the AOT is fixed to 0.25 at 0.670 μm. The aerosols are well mixed between 0 and 3 km. The surface BPDF is parameterized using the FRS surface model. We have a set of measurements for each surface class. The calculations are made in the principal plan for a sun zenith angle of 50°. We restrict the scattering angle range between 80° and 160°, which is an angle range typically observed from downward-looking passive sensors. The angular resolution is less than 1.5° as for the RSP instrument. These simulations constitute the input of the algorithm. In the retrieval scheme (optimal method estimate), the polarized reflectances are simulated using the three other surface BPDF models tested in this study (VB, FR, and NB). Table 3 shows the differences obtained for the AOT, the effective radius, the real part of the refractive index, and the single scattering albedo.

Table 3. Differences on the Retrieved Aerosol Parameters When Using the VB, FR, and NB Surface Models to Fit Polarized Reflectances Measurements Simulated with the FRS Surface Model

Models/ Parameters	ΔAOT at 0.670 μm	Δr_{eff} (μm)	Δm_r	$\Delta\omega_0$ at 0.670 μm
$0.40 < \text{NDVI} < 0.45$				
VB	0.082	0.026	0.130	0.180
FR	0.082	0.025	0.110	0.145
NB	0.008	0.001	0.010	0.014
$0.88 < \text{NDVI} < 0.89$ and Total Reflectance at 2.2 μm < 0.05				
VB	0.050	0.019	0.200	0.100
FR	0.018	0.007	0.032	0.070
NB	0.003	0.0001	0.003	0.007

The results shown in Table 3 confirm that the VB and FR models should not be used for the purpose of defining the BPDF of a target. In particular, the use of the VB model instead of the FRS one leads to large differences on the aerosol parameters for both surface classes. The differences observed for the AOT, the aerosol single scattering albedo, and the real part of the refractive index are notably larger than the retrieval requirements suggested by Mishchenko *et al.* [39] for climate research over land. The differences observed on the aerosol parameters for the NB model are small. For the 0.40–0.45 NDVI class, we observed relative differences of approximately 3% and 1.5%, respectively, for the AOT and the single scattering albedo. The differences observed for the 0.88–0.89 NDVI class were negligible.

5. Conclusion

We have presented experimental results for the polarization generated by vegetated surfaces in the spectral range from 0.67 to 2.2 μm. The measurements were performed on board a lightweight aircraft, close to the principal plane (±20°), for sun zenithal angles varying between 46° and 60° and for a range of scattering angles varying between 75° and 145°. We used aerosol properties and optical thicknesses collected by a sun photometer that was located close to the track of the aircraft in order to perform the atmospheric correction. The observed surfaces mainly correspond to forested areas and closely cropped farmlands. Our results confirm that the polarization generated by reflection of vegetated surfaces can be understood as being primarily a specular reflection process, at least over the scattering angle range sampled in this study (<145°). It was observed that the observations at 0.67, 0.87, and 1.6 μm were strongly correlated with the observations at 2.2 μm.

It is not possible from our measurements to see any spectral dependence of the surface polarization in the given spectral channels. We found that a linear combination of the theoretical models developed for bare soil and vegetation [17] is not adequate to fit the observed surface polarization angular behavior. The use of this model leads to significant errors on the retrieved aerosol parameters. The model developed for the analysis of the POLDER measurements [21] allows the observed angular behavior to be reproduced quite well when it is adjusted with observations at 2.2 μm. However, when the parameters developed for global use are used, it overestimates the surface-polarized reflectance between 0.25×10^{-3} and 3.5×10^{-3} for the area where the measurements were made and for closely cropped surfaces. We also observed that the surface-polarized reflectance can still be robustly modeled by only considering the Fresnel reflectance and the observations at 2.2 μm. This simple model can be improved by correcting the polarized reflectance by a factor that accounts for the effects of shadowing. Note that such a model can be easily implemented in transfer radiative codes, where the surface reflection matrix is filled out according to the Fresnel's law and simply multiplied by a factor. In particular, it can be used to accurately calculate the diffuse interactions between the surface and the atmosphere. The relative differences on the aerosol parameters retrieved with the scaled Fresnel reflectance with shadowing (FRS) model and the model developed by Nadal and Bréon [21] do not exceed 3%.

In terms of what is required for a surface BPDF model that can be used in aerosol retrievals using polarized reflectance measurements, observations at long wavelengths such as 1.6 or 2.2 μm are highly desirable in order to allow the parameters that define the surface and the atmospheric properties to be retrieved at the same time. From our data, the FRS model and the one developed by Nadal and Bréon [21] are similar in performance, provided long wavelength measurements are available to constrain them. We therefore anticipate that additional observations at long wavelengths will allow significant improvements in the modeling of polarized observations made over land. The multispectral polarized capabilities of the future Glory Aerosol Polarimetry Sensor [40] should therefore enhance our ability to detect aerosols over land and to monitor their effects on climate and air quality.

The authors acknowledge C. Verwaerde, J.-Y. Balois, and P. François for their work on the MICROPOL instrument and for the realization of the flights. F. Waquet is grateful to the Région Nord-Pas de Calais, le Centre National d'Etudes Spatiales (CNES) and the Université des Sciences et Technologies de Lille (USTL) for funding his postdoctoral appointment.

References

1. P. Forster, V. Ramaswamy, P. Artaxo, T. Berntsen, R. Betts, D. W. Fahey, J. M. Haywood, J. Lean, D. C. Lowe, G. Myhre, J. Nganga, R. Prinn, G. Raga, M. Schulz, and R. Van Dorland, "Changes in atmospheric constituents and in radiative forcing," in *Climate change 2007: The Physical Basis. Contribution of Working Group I to the Fourth Assessment Report of the Intergovernmental Panel on Climate Change*, S. Solomon, D. Qin, M. Manning, Z. Chen, M. Marquis, K. B. Averyt, M. Tignor, and H. L. Miller, eds. (Cambridge University, 2007).
2. M. D. King, Y. J. Kaufman, D. Tanré, and T. Nakajima, "Remote sensing of tropospheric aerosols from space: past present and future," Bull. Am. Meteorol. Soc. **80**, 2229–2259 (1999).
3. Y. J. Kaufman, D. Tanré, and O. Boucher, "A satellite view of aerosols in the climate system," Nature **419**, 215–223 (2002).
4. R. S. Fraser and Y. J. Kaufman, "The relative importance of aerosol scattering and absorption in remote sensing," IEEE Trans. Geosci. Remote Sens. **GE-23**, 625–633 (1985).
5. C. Popp, A. Hauser, N. Foppa, and S. Wunderle, "Remote sensing of aerosol optical depth over central Europe from MSG-SEVIRI data and accuracy assessment with ground-based AERONET measurements," J. Geophys. Res. **112**, D24S11 (2007).
6. Y. J. Kaufman and C. Sendra, "Algorithm for automatic atmospheric corrections to visible and near-IR satellite imagery," Int. J. Remote Sens. **9**, 1357–1381 (1988).
7. Y. J. Kaufman, D. Tanré, L. A. Remer, E. F. Vermote, A. Chu, and B. N. Holben, "Operational remote sensing of tropospheric aerosol over land from EOS moderate resolution imaging spectroradiometer," J. Geophys. Res. **102**, 17051–17067 (1997).
8. Y. J. Kaufman, A. E. Wald, L. A. Remer, B.-C. Gao, R.-R. Li, and L. Flynn, "The MODIS 2.1 μm channel correlation with visible reflectance for use in remote sensing of aerosol," IEEE Trans. Geosci. Remote Sens. **35**, 1286–1298 (1997).
9. Y. J. Kaufman, N. Gobron, B. Pinty, J.-L. Widlowski, and M. M. Verstraete, "Relationship between surface reflectance in the visible and mid-IR used in MODIS aerosol algorithm —theory," Geophys. Res. Lett. **29**, 2116 (2002).
10. F. Waquet, P. Goloub, J.-L. Deuzé, J.-F. Léon, F. Auriol, C. Verwaerde, J.-Y. Balois, and P. François, "Aerosol retrieval over land using a multiband polarimeter and comparison with path radiance method," J. Geophys. Res. **112**, D11214 (2007).
11. A. D. de Almeida Castanho, R. Prinn, J. V. Martins, M. Herold, C. Ichoku, and L. T. Molina, "Analysis of visible/SWIR surface reflectances ratios for aerosol retrievals from satellite in Mexico City urban area," Atmos. Chem. Phys. **7**, 5467–5477 (2007).
12. L. A. Remer, Y. J. Kaufman, D. Tanré, S. Mattoo, D. A. Chu, J. V. Martin, R.-R. Li, C. Ichoku, R. C. Levy, R. G. Kleidman, T. F. Eck, E. Vermote, and B. N. Holben, "The MODIS aerosol algorithm, products, and validation," J. Atmos. Sci. **62**, 947–973 (2005).
13. R. J. Flowerdew and J. D. Haigh, "An approximation to improve accuracy in the derivation of surface reflectances from multi-look satellite radiometers," Geophys. Res. Lett. **22**, 1693–1696 (1995).
14. J. P. Veefkind, G. de Leeuw, and P. A. Durkee, "Retrieval of aerosol optical depth over land using two-angle view satellite radiometry during TARFOX," Geophys. Res. Lett. **25**, 3135–3138 (1998).
15. P. R. North, "Estimation of aerosol opacity and land surface bidirectional reflectance from ATSR-2 dual angle imagery: operational method and validation," J. Geophys. Res. **107**, 4149 (2002).
16. D. J. Diner, J. V. Martonchik, R. A. Kahn, B. Pinty, N. Gobron, D. L. Nelson, and B. N. Holben, "Using angular and spectral

shape similarity constraints to improve MISR aerosol and surface retrievals over land," Remote Sens. Environ. **94**, 155–171 (2005).
17. F. M. Bréon, D. Tanré, P. Lecomte, and M. Herman, "Polarized reflectance of bare soils and vegetation: measurements and models," IEEE Trans. Geosci. Remote Sens. **33**, 487–499 (1995).
18. J. L. Deuzé, F. M. Bréon, P. Y. Deschamps, C. Devaux, M. Herman, A. Podaire, and J. L. Roujean, "Analysis of the POLDER (POLarization and Directionnality of Earth's Reflectances) airborne instrument observations over land surfaces," Remote Sens. Environ. **45**, 137–154 (1993).
19. B. Cairns, L. D. Travis, and E. E. Russel, "An analysis of polarization: ground-based upward looking and aircraft/satellite-based downward looking measurements," in *Satellite Remote Sensing of Clouds and the Atmosphere II* (SPIE, 1998), pp. 103–114.
20. G. Rondeaux and M. Herman, "Polarization of light reflected by crop canopies," Remote Sens. Environ. **38**, 63–75 (1991).
21. F. Nadal and F. M. Bréon, "Parametrisation of surface polarised reflectance derived from POLDER spaceborne measurements," IEEE Trans. Geosci. Remote Sens. **37**, 1709–1718 (1999).
22. F. Waquet, J.-F. Léon, P. Goloub, J. Pelon, D. Tanré, and J.-L. Deuzé, "Maritime and dust aerosol retrieval from polarized and multispectral active and passive sensors," J. Geophys. Res. **110**, D10510 (2005).
23. B. Cairns, L. Travis, M. I. Mishchenko, and J. Chowdhary, "Aerosol retrievals over land surfaces: the advantages of polarization," *Proceedings of AMS Annual Meeting*, Albuquerque, N.M., January 2001.
24. T. Elias, B. Cairns, and J. Chowdhary, "Surface optical properties measured by the airborne research scanning polarimeter during the CLAMS experiment," Proc. SPIE **5235**, 595–606 (2004).
25. B. Cairns, L. D. Travis, and E. E. Russel, "The research scanning polarimeter: calibration and ground-based measurements," Proc. SPIE **3754**, 186–196 (1999).
26. J.-L. Deuzé, F.-M. Bréon, C. Devaux, P. Goloub, M. Herman, B. Lafrance, F. Maignan, A. Marchand, F. Nadal, G. Perry, and D. Tanré, "Remote sensing of aerosols over land surfaces from POLDER-ADEOS-1 polarized measurements," J. Geophys. Res. **106**, 4913–4926 (2001).
27. G. Schaepman-Strub, M. E. Schaepman, T. H. Painter, S. Dangel, and J. V. Martonchik, "Reflectance quantities in optical remote sensing definitions and case studies," Remote Sens. Environ. **103**, 27–42 (2006).
28. J. E. Hansen and L. D. Travis, "Light scattering in planetary atmospheres," Space Sci. Rev. **16**, 527–610 (1974).
29. J.-L. Deuzé, M. Herman, and R. Santer, "Fourier series expansion of the transfer equation in the atmosphere-ocean system," J. Quant. Spectrosc. Radiat. Transfer **41**, 483–494 (1989).
30. O. Dubovik and M. D. King, "A flexible inversion algorithm for retrieval of aerosol optical properties from sun and sky radiance measurements," J. Geophys. Res. **105**, 20673–20696 (2000).
31. B. Lafrance, "Simplified model of the polarized light emerging from the atmosphere. Correction of the stratospheric aerosol impact on POLDER measurements" (in French), Ph.D. thesis (Université des Sciences et Techniques de Lille, France, 1997).
32. K. Coulson, G. Bouricius, and E. Gray, "Optical reflection properties of natural surfaces," J. Geophys. Res. **70**, 4601–4611 (1965).
33. V. C. Vanderbilt, L. Grant, L. L. Biehl, and B. F. Robinson, "Specular, diffuse, and polarized light scattered by two wheat canopies," Appl. Opt. **24**, 2408–2418 (1985).
34. P. M. Saunders, "Shadowing on the ocean and the existence of the horizon," J. Geophys. Res. **72**, 4643–4649 (1967).
35. O. P. Hasekamp and J. Landgraf, "Retrieval of aerosol properties over land surfaces: capabilities of multiple-viewing-angle intensity and polarization measurements," Appl. Opt. **46**, 3332–3344 (2007).
36. J.-F. Léon, P. Chazette, and F. Dulac, "Retrieval and monitoring of aerosols optical thickness over an urban area using spaceborne and ground-based remote sensing," Appl. Opt. **38**, 6918–6926 (1999).
37. J. B. Pollack, O. B. Toon, and B. N. Khare, "Surface refractive index," Icarus **19**, 372–389 (1973).
38. F. Waquet, B. Cairns, K. Knobelspiesse, J. Chowdhary, L. D. Travis, B. Schmid, and M. I. Mishchenko, "Polarimetric remote sensing of aerosols over land," J. Geophys. Res. **114**, D01206.
39. M. I. Mishchenko, M. I. B. Cairns, J. E. Hansen, L. D. Travis, R. Burg, Y. J. Kaufman, J. V. Martins, and E. P. Shettle, "Monitoring of aerosol forcing of climate from space: analysis of measurement requirements," J. Quant. Spectrosc. Radiat. Transfer **88**, 149–161, doi: 10.1016/.jqsrt.2004.03030 (2004).
40. M. I. Mishchenko, B. Cairns, G. Kopp, C. F. Schueler, B. A. Fafaul, J. E. Hansen, R. J. Hooker, T. Itchkawich, H. B. Maring, and L. D. Travis, "Accurate monitoring of terrestrial aerosols and total solar irradiance: introducing the Glory mission," Bull. Am. Meteorol. Soc. **88**, 677–691 (2007).